Personal and Ubiquitous Computing (2022) 26:1–10
https://doi.org/10.1007/s00779-020-01492-2

ORIGINAL ARTICLE

Synergic deep learning model–based automated detection and classification of brain intracranial hemorrhage images in wearable networks

C. S. S. Anupama[1] · M. Sivaram[2] · E. Laxmi Lydia[3] · Deepak Gupta[4] · K. Shankar[5]

Received: 24 September 2020 / Accepted: 16 November 2020 / Published online: 23 November 2020

Abstract
With an intention of improving healthcare performance, wearable technology products utilize several digital health sensors which are classically linked into sensor networks, including body-worn and ambient sensors. On the other hand, intracerebral hemorrhage (ICH) defines the injury of blood vessels in the brain regions, which is accountable for 10–15% of strokes. X-ray computed tomography (CT) scans are commonly employed to determine the position and size of the hemorrhages. Manual segmentation of the CT scans by planimetry using a radiologist is effective; however, it consumes more time. Therefore, this paper develops deep learning (DL)–based ICH diagnosis using GrabCut-based segmentation with synergic deep learning (SDL), named GC-SDL model. The proposed method make use of Gabor filtering for noise removal, thereby the image quality can be raised. In addition, GrabCut-based segmentation technique is applied to identify the diseased portions effectively in the image. To perform the feature extraction process, SDL model is utilized and finally, softmax (SM) layer is employed as a classifier. In order to investigate the performance of the GC-SDL model, an extensive set of experimentation takes place using a benchmark ICH dataset, and the results are examined under different evaluation metrics. The experimental outcome stated that the GC-SDL model has reached a higher sensitivity of 94.01%, specificity of 97.78%, precision of 95.79%, and accuracy of 95.73%.

Keywords Wearable sensors · Medical imaging · Deep learning · Segmentation · ICH · Classification

1 Introduction

With the introduction of wearable network technologies, smart healthcare is progressively increased. The real-time healthcare monitoring system needs to be safe, efficient, and patient-centered [1]. Wearable devices, like smartwatch and fitness band, become an important part of human lives. Generally, the wearables are worn incessantly through the day and thus offer a chance of gathering details related to the clients with the unprecedented stages. Additionally, several wearables are directly worn over the skin, and they may include sensors not available on common smartphones, which are useful for medical diagnosis [2]. In general, intracerebral hemorrhage (ICH) is defined as a neurological disease that results in blood vessel damage and infected tissue, and it is gradually extended to the brain ventricles. The application of X-ray and computed tomography (CT) scanning models are highly beneficial for physicians to define the features of the disease, and it helps to provide the treatment accordingly. When compared to X-ray, the CT scan method is applied extensively and prominently in order to diagnose the patients

✉ K. Shankar
drkshankar@ieee.org

C. S. S. Anupama
cssanupama@gmail.com

M. Sivaram
sivaram.murugan@lfu.edu.krd

E. Laxmi Lydia
elaxmi2002@yahoo.com

Deepak Gupta
deepakgupta@mait.ac.in

[1] V.R.Siddhartha Engineering College, Vijayawada, India

[2] Research Center, Lebanese French University, 44001 Erbil, Iraq

[3] Computer Science and Engineering, Vignan's Institute of Information Technology (Autonomous), Visakhapatnam, India

[4] Department of Computer Science & Engineering, Maharaja Agrasen Institute of Technology, Delhi, India

[5] Department of Computer Applications, Alagappa University, Karaikudi, India

infected with ICH. Moreover, it shows the area of ICH which is a major diagnostic objective of stroke intensity, long-term functional result, and fatality. ICH volume change is a typical effect and secondary result in clinical trials. Additionally, the position of ICH affects the processing results in patients with stroke. Hence, quantitative metrics of ICH like volume, position, as well as structure are considered as major factors for treatment and alternate medical decisions.

Initially, ICH volume is determined robustly, for instance, ABC/2 model. Here, the user selects the slice with maximum hemorrhage. The length of an intersection among initial axis and hemorrhage are implied as A. Followed by, an orthogonal line has to be developed at the intermediate position of length A with maximum hemorrhage. Hence, the length of intersection from the second orthogonal axis and hemorrhage is represented as B. In this scenario, the reader validates the count of slices where hemorrhage exists (C). Thus, volume estimation is depicted by $A \times B \times C$ 2, which is assumed to be the approximate value of volume estimation where it is meant to be an ellipsoid structure. As the model is simple and elegant to execute, it is applied widely and robustly for rapid volume estimation. Even though ABC/2 is applied vastly [3], referred that the estimated error related to the ABC/2 model is higher when compared with planimetry that needs slice-by-slice hemorrhage segmentation by well-trained readers.

From the abovementioned statement, planimetry consumes maximum time and manpower; however, it is effective in generating précised ICH area than the ABC/2 method, particularly for the irregular structure of ICH and lower thickness (high resolution) scans. An alternate problem is that ICH is changed periodically. The structure of ICH has to be defined first; however, the approximation might become inaccurate in the time since the lesion gets changed in shape and texture, also it shifts by surrounding tissues. Surgical inventions that aim in eliminating the ICH are also capable of changing the ICH shape and results in excess bleeding. Additionally, the ABC/2 approach has depicted consistently overestimate infarct volume and is composed of an important interrater difference. Hence, a robust, independent, and valid model for determining the place of hemorrhage and its volume from CT scans is related in clinical trials. Here, accuracy can be achieved by the enhanced diagnostic and prognostic value. Also, many other approaches have been projected ICH segmentation with the help of magnetic resonance images (MRI) [4]. Moreover, MRI sequences as well as protocols differ in sites, and no general, remarkable, MRI protocol for ICH standard-of-care. Hence, the ICH segmentation has to be performed on the basis of CT scan details which is scalable, reproducible, accessible, and verified over planimetry.

In the last decade, the machine learning (ML) method has been developed progressively that has increased processing efficiency and collection of big data [5]. Advancements in image identification have relied on deep learning (DL), which belongs to ML that guides in modifying the landscape of medical by reaching physician-level performance in diverse operations. Such breakthroughs maximize the diagnostic precision, streamline physician workflow, offer expertise to learn populations, and intend to develop novel biological insights. Regardless, the requirement to big data as well as black-box problem acts as substantial barriers while developing clinical DL modules [6]. The major issue in creating medical imaging DL systems is that large-scale datasets could not be accessed.

Here, DL method is one of the well-known and potential in examining useful patterns from actual data with no explicit directions. In order to improve the ability, earlier medical imaging DL works have gained physician-level performance under 100,000 images for training the system. Thus, accumulating and modeling large datasets are onerous and impossible for developers. In addition, institutions hesitate to distribute the data with physical collaborators as the patient security and ethical considerations are significant. Even though, the developer attempts to gather massive datasets, labeling and verifying big data are costlier and time-consuming [7–9]. Secondly, the problem is which the interior workings and decision-making models of the ML model are still challenging [10]. The US Food and Drug Administration needs clinical decision support software for defining the rationale where it allows the users to review the suggestions. The condition is satisfied by gaining trust from physicians, medical DL models ought to provide explanations for the outputs. These problems have to be resolved for training and clinical implementation serves as developing clinician adoption of the DL method in clinical practice [10].

Prevedello et al. [11] projected 2 models relied on convolutional neural networks (CNNs). Among these 2 models, the first one concentrates on predicting ICH, mass effect, and hydrocephalus while scanning the ICH, whereas the second one is applied for detecting malicious acute infarcts. Then, overall CT scans have been applied for training, verification, and also for testing. These 2 models are related to CNN with recurrent neural network (RNN) which is presented for detecting ICH. Grewal et al. [12] deployed a 40-layer CNN, named as DenseNet, with a bidirectional long short-term memory (Bi-LSTM) layer to the purpose of ICH prediction. Moreover, 3 auxiliary operations were presented for the dense convolutional block for preceding the binary segmentation of ICH sites. These tasks are composed of a single convolutional layer and a deconvolution layer for computing upsampling feature maps to actual image size. The LSTM layer is included in interslice dependencies of CT scans in every subject.

Ye et al. [13] projected a 3D joint convolutional and RNN (CNN-RNN) for predicting and classifying ICH regions. VGG-16 has been employed as the CNN model, and the bidirectional gated recurrent unit (GRU) was applied as an RNN technique. RNN layer performs similar to slice interpolation

model provided by Lee et al. [14]; however, it is flexible by means of closer slices in the classification. Among all other methodologies, the CNN approach was tailored for computing CT slices simultaneously [15]. Jnawalia et al. [16] presented an ensemble of 3 diverse CNN schemes for predicting ICH. The CNN models depend upon the structure of AlexNet and GoogleNet which are expanded to a 3D technique by consuming all slices. Furthermore, a minimum count of parameters and filter specifications are considered.

In Arbabshirani et al. [17], an ensemble of 3D CNN approaches with an input has been executed and estimated under the application of retrospective as well as prospective CT scans. A maximum AUC is accomplished on the retrospective study, and maximum sensitivity as well as specificity have been accomplished on testing datasets. In line with this, the transfer learning on an ensemble of 4 familiar CNN methods for predicting ICH subtypes as well as bleeding points. The 4 methods are VGG-16, ResNet-50, Inception-v3, and Inception-ResNet-v2. The spatial dependency among closer slices is considered by developing a slice interpolation technique. This ensemble approach undergoes training and validations with the help of a dataset with CT scans and sampled by applying a retrospective dataset with 200 CT scans and a prospective dataset with 200 scans. Thus, the ICH detection model has provided higher AUC, sensitivity, and specificity. But, the model has generated minimum sensitivity for classifying ICH subtypes with considerable sensitivity and specificity. Also, the least sensitivity was addressed for EDH slices in the retrospective test set and manageable value for IPH slices in the prospective test set. The entire localization accuracy of attention maps is at maximum from model segmentation and radiologists' maps of bleeding points.

A new CNN model for the identification of intraparenchymal, epidural/subdural, and subarachnoid hemorrhages on noncontrast CT has been provided in [18]. Besides, Majumdar et al. [19] introduced DCNN for concurrently perform feature extraction and classification, removing the many handcrafted processes. The results are enhanced by the determination of the mean output for rotations of the input image. Though several ICH diagnosis models are available in the literature, only less number of studies have focused on the DL models. In addition, the ICH diagnosis model in the wearable network environment becomes essential to assist medical services to remote areas.

This paper develops a DL-based ICH diagnosis using GrabCut-based segmentation with synergic deep learning (SDL), named the GC-SDL model. The GC-SDL model involves a set of processes namely preprocessing, segmentation, feature extraction, and classification. Initially, the Gabor filtering (GF) technique is applied as a preprocessing technique to eradicate the noise. Followed by, GrabCut-based segmentation technique is applied to identify the diseased portions effectively in the preprocessed image. Next to that, the SDL based feature extraction process takes place to attain a useful set of feature vectors. At last, the softmax (SM) layer is employed for the classification process to determine the different classes of ICH. For validation, a series of experiments are carried out on the ICH dataset.

2 The proposed GC-SDL model

The proposed ICH diagnosis model, named GC-SDL model comprises GF-based preprocessing, GrabCut-based segmentation, SDL-based feature extraction, and SM-based classification. The working principle of the GC-SDL model is shown in Fig. 1, and the processes are detailed in the subsequent sections.

2.1 Image preprocessing

Gabor filter is a linear filtering technique employed to analyze the feature, which examines whether there are some particular frequency details in the image in particular ways in a localized region over the point of analysis. The impulse response is described by a sinusoidal wave (a plane wave for 2D Gabor filters) which is enhanced by a Gaussian function. Due to the multiplication-convolutional feature, the Fourier transform (FT) of harmonic function (sinusoidal function) as well as FT of Gaussian function are considered. A filter is composed of the real and imaginary module which represents the orthogonal directions.

The 2 modules might be developed as complex and real numbers, as given below.

$$g(x,y;\lambda,\theta,\psi,\sigma,\gamma) = \exp\left(\frac{x'^2+\gamma^2y'^2}{2\sigma^2}\right)\exp\left(i\left(2\pi\frac{x'}{\lambda}+\psi\right)\right) \quad (1)$$

$$g(x,y;\lambda,\theta,\psi,\sigma,\gamma) = \exp\left(\frac{x'^2+\gamma^2y'^2}{2\sigma^2}\right)\cos\left(i\left(2\pi\frac{x'}{\lambda}+\psi\right)\right) \quad (2)$$

$$g(x,y;\lambda,\theta,\psi,\sigma,\gamma) = \exp\left(\frac{x'^2+\gamma^2y'^2}{2\sigma^2}\right)\sin\left(i\left(2\pi\frac{x'}{\lambda}+\psi\right)\right) \quad (3)$$

where $x' = xcos\theta + ysin\theta$ and $y' = -xsin\theta + ycos$. Here, λimplies the wavelength of sinusoidal factor, θ denotes the direction of normal to parallel stripes of a Gabor function, ψrefers the phase offset, σ represents the sigma/SD of Gaussian envelope and γmeans the spatial aspect ratio, and shows the ellipticity of Gabor function.

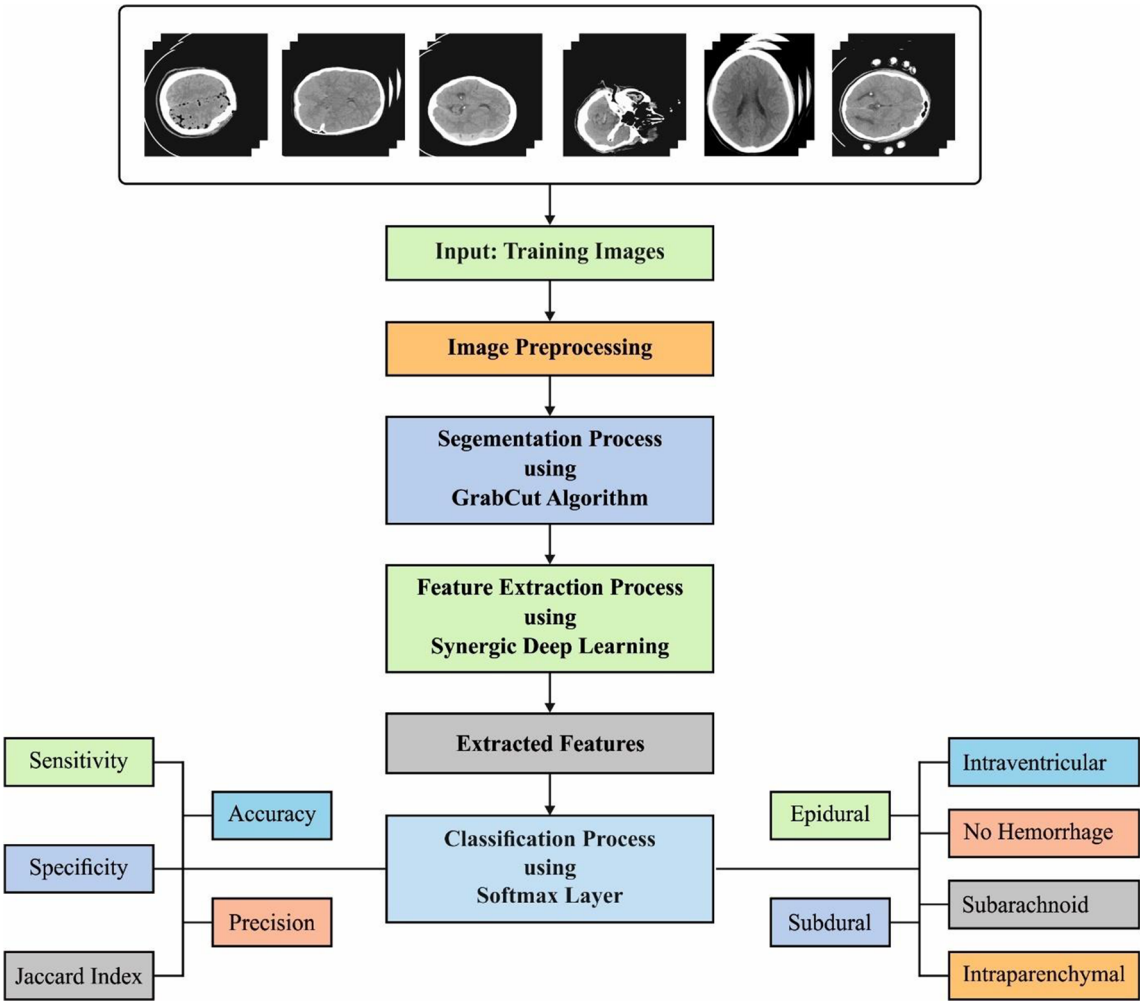

Fig. 1 Overall process of GC-SDL

2.2 Image segmentation

In this study, GrabCut segmentation is used to segment the preprocessed image. The developers have presented a model for identifying a binary segmentation (background and foreground) of an image by formalizing an energy reduction model, and expanded by applying color instead of just grayscale details. The color image I, and array $z = (z_1, \ldots, z_n, \ldots, z_N)$ of N pixels where $z_i = (R_i, G_i, B_i)$, $i \in [1, \ldots, N]$ in RGB space. In segmentation is meant to be an array $\alpha = (\alpha_1, \ldots \alpha_N)$, $\alpha_i \in \{0, 1\}$, which allocates the label for all pixels in an image which comes under the background or foreground. The trimap T is illustrated by a user—in a semiautomated direction with 3 regions: T_B, T_F, and T_U, where each one has a background, foreground, and uncertain pixels, correspondingly. Pixels from T_B and T_F are clamped as background and foreground correspondingly that refers that GrabCut is not applicable for such labels, while the pixels from T_U are suitable for labeling. Color information is developed by Gaussian mixture models (GMMs). A complete covariance GMM of K elements are described to background pixels ($\alpha_i = 0$), and the foreground pixels ($\alpha_j = 1$), are parametrized as follows

$$\theta = \{\pi(\alpha, k), \mu(\alpha, k), \Sigma(\alpha, k), \alpha \in \{0, 1\}, k = 1..K\}, \quad (4)$$

where π is a weight, μ implies the mean, and Σ refers to the covariance matrices. Also, the array $k = \{k_1, k_i, \ldots k_N\}$, $k_i \in \{1, \ldots K\}$, $i \in [1, N]$ which means the element of background or foreground GMM (based on α_i) the pixel z_i. The energy function for segmentation is expressed as,

$$E(\alpha, k, \theta, z) = U(\alpha, k, \theta, z) + V(\alpha, z), \quad (5)$$

where U denotes the possibility potential, relying on probability distributions p of the GMM:

$$U(\alpha, k, \theta, z) = \sum_i -\log p(z_i|\alpha_i, k_i, \theta) - \log \pi(\alpha_i, k_i) \quad (6)$$

and V represents a regularizing prior to considering the segregated regions which are coherent by means of color, that assumes a neighborhood C over each pixel

$$V(\alpha, z) = \gamma \sum_{\{m,n\} \in C} [\alpha_n \neq \alpha_m] \exp\left(-\beta \|z_m - z_n\|^2\right) \quad (7)$$

Using the energy minimization model and initial trimap T, the last segmentation is conducted under the application of a minimum cut algorithm. Figure 2 shows the process in GrabCut model.

2.3 Feature extraction

The SDL model extracts the useful set of features from the segmented image. It is represented by SDL^k with 3 main units such as input layer, k DCNN components and C_k^2 synergic network (SN) [20]. The entire SDL approach is demonstrated in Fig. 3. Every deep convolutional neural network (DCNN) element of a network provides an autonomous learning representation from data with appropriate input data.

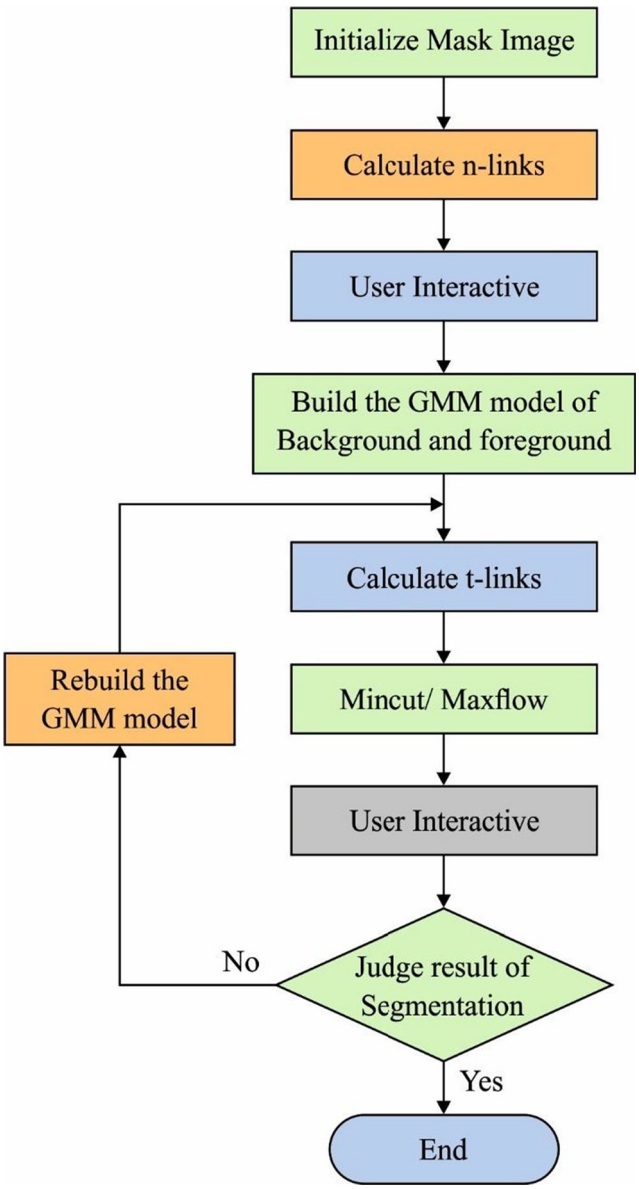

Fig. 2 Process in GrabCut algorithm

The SN is composed of a process with fully connected (FC) architecture to make sure whether the input layer belongs to an identical class and provides remedial comment on the application of a synergic error. Then, the SDL approach is divided into 3 submodules.

2.3.1 Pair input layer

Unlike previous DCNN, the proposed SDL^k method gets n input data that is trained in a random fashion. Every group of 200 data with a class label is induced as an input for DCNN units, and the pair is comprised of a comparative synergic label which is presented by SN. The uniform size is retained by reforming images as $224 \times 224 \times 3$ under the application of bicubic interpolation.

2.3.2 DCNN component

Because of the implicit nature of the important residual network (ResNet), a ResNet − 50 could be applied for initializing every DCNN components as DCNN − a ($a = 1, 2, \ldots, n$). Hence, it is pointed out that a kind of DCNN, such as AlexNet, GoogLeNet, and VGGNet are suited in the SDL method as DCNN unit. Such elements are trained with the help of data sequence $X = \{x^{(1)}, x^{(2)}, \ldots, x^{(M)}\}$ and final class label series $Y = \{y^{(1)}, y^{(2)}, \ldots, y^{(M)}\}$,intends to proceed with the set of variables θ which undergoes cross-entropy loss as shown below.

$$log(\theta) = -\frac{1}{M}\left[\sum_{a=1}^{M}\sum_{b=1}^{K} 1\left\{y^{(1)} = b\right\} log \frac{e^{Z_b^{(a)}}}{\sum_{l=1}^{K} z_l^{(a)}}\right] \quad (8)$$

where n implies the class count, $Z^{(a)} = F(x^{(a)}, \theta)$ denotes the forward computing. An obtained variable set to DCNN−a is implied as θ^a, and the variables do not share massive DCNN components.

2.3.3 SDL model

The DCNN element with synergic labels of pair is applied for FC learning, embedding, and input layers. Consider a data pair (Z_A, Z_B), which is fed as input to the two DCNN elements such as (DCNNa, DCNNb), respectively. The final result from the consecutive FC layer in a *DCNN* represents the deep data features that are learned by DCNN retrieved from forward computing, as depicted below.

$$f_A = \mathcal{F}\left(Z_A, \theta^{(a)}\right) \quad (9)$$

$$f_B = \mathcal{F}\left(Z_B, \theta^{(a)}\right) \quad (10)$$

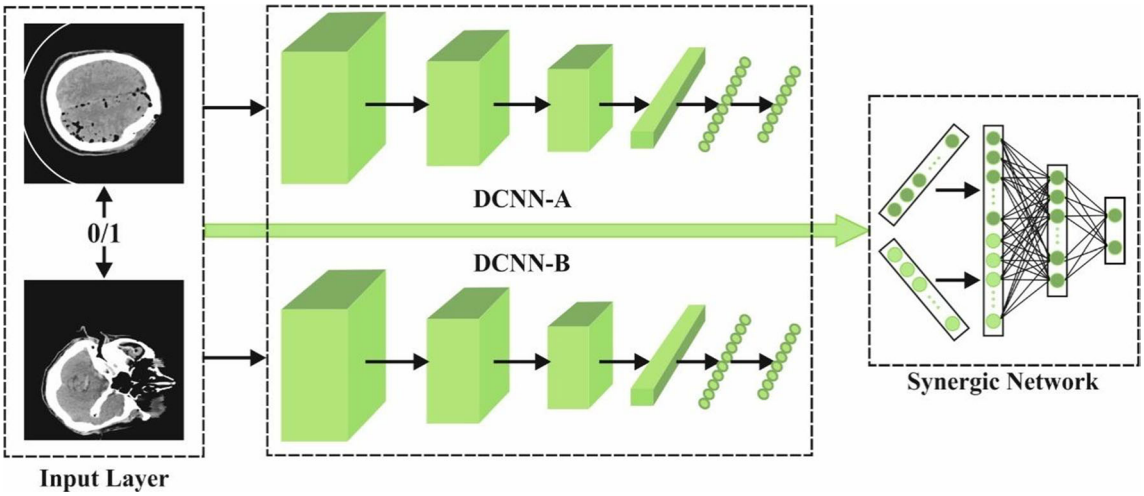

Fig. 3 Architecture of SDL

Then, the deep features from all data are embedded using $f_{A\circ B}$, and certain outcomes with the synergic label is demonstrated as given.

$$ys(Z_A, Z_B) = \begin{cases} 1 & if \quad y_A = y_B \\ 0 & if \quad y_A \neq y_B \end{cases} \tag{11}$$

In order to overcome the challenging issues, the percentage data pair in a class is higher, and it is simple for viewing the synergic signal by alternate sigmoid layer, and succeeding binary cross-entropy loss is represented below

$$l^S\left(\theta^S\right) = y_S \log \widehat{y_S} + (1-y_S)\log\left(1-\widehat{y_S}\right) \tag{12}$$

where θ^S denotes the attribute of the SN, $\widehat{y_S}$ implies the forward computing of SN. It validates that if the input data pair comes under the same class and offer the remedial response on the existence of the synergic error.

2.3.4 Training and testing

Once the training is done, the attribute of DCNN elements and SN is maximized as follows.

$$\begin{cases} \theta^{(a)}(z+1) = \theta^{(a)}(z) - \eta(z).\Delta^{(a)} \\ \theta^{S(a)}(z+1) = \theta^{S(a)}(z) - \eta(z).\Delta^{S(a,b)} \end{cases} \tag{13}$$

where $\eta(z)$ and $S(a, b)$ refers rate of learning and SN among *DCNNa* and *DCNNb* is represented under.

$$\Delta^{(a)} = \frac{\partial l^{(a)}\left(\theta^{(a)}\right)}{\partial \theta^{(a)}} + \succ \sum_{b=1, b\neq a}^{n} \frac{\partial l^{S(a)}\left(\theta^{S(a,b)}\right)}{\partial \theta^{S(a,b)}} \tag{14}$$

$$\Delta^{S(a)} = \frac{\partial l^{S(a)}\left(\theta^{S(a,b)}\right)}{\partial \theta^{S(a,b)}} \tag{15}$$

and $\succ$signifies the tradeoff among submodel of classification as well as synergic error. The consolidation of the training process of the SDL^2 the model has been maximized. Under the application of trained SDL^k, the test data x is classified as DCNN component $\mathrm{DCNN}-u$ where it has provided a prediction vector $P^{(a)} = \left(p_1^{(a)}, p_2^{(a)}, \ldots, p_k^{(a)}\right)$, activation in the consequent FC layer. The class labels of test data are predicted and implied as,

$$y(Z) = \underset{v}{\text{argmax}} \left\{ \sum_{u=1}^{k} p_1^{(u)}, \ldots, \sum_{u=1}^{k} p_v^{(u)}, \ldots, \sum_{u=1}^{k} p_K^{(u)} \right. \tag{16}$$

2.4 Image classification

Once the feature vectors are extracted, the classification process takes place to identify the different class labels using the SM layer. It is defined as a classifier applied to multilabel classification problems. It precedes a mapping function for the input vector c from N-dimensional space to K class labels, as illustrated under.

$$v_q = \frac{\exp\left(\theta_q^Z \mathrm{c}\right)}{\sum_{\mathrm{k}=1}^{\mathrm{K}} \exp\left(\theta_{\mathrm{k}}^Z \mathrm{c}\right)} (q = 1, 2, \ldots \mathrm{K}) \tag{17}$$

where $\theta_k = [\theta_{k1}\theta_{k2}\ldots\theta_{kN}]^Z$ means the weights, which are tuned under the application of an efficient optimization model.

3 Performance validation

The proposed model is simulated using Python—3.6.5, Python Packages tensorflow (GPU-CUDA Enabled), keras, numpy, pickle, matplotlib, sklearn, pillow, and opencv-python. To estimate the performance of the presented method, an experimental analysis performs utilizing a benchmark ICH dataset [21]. Figure 4 illustrates the sample group of images

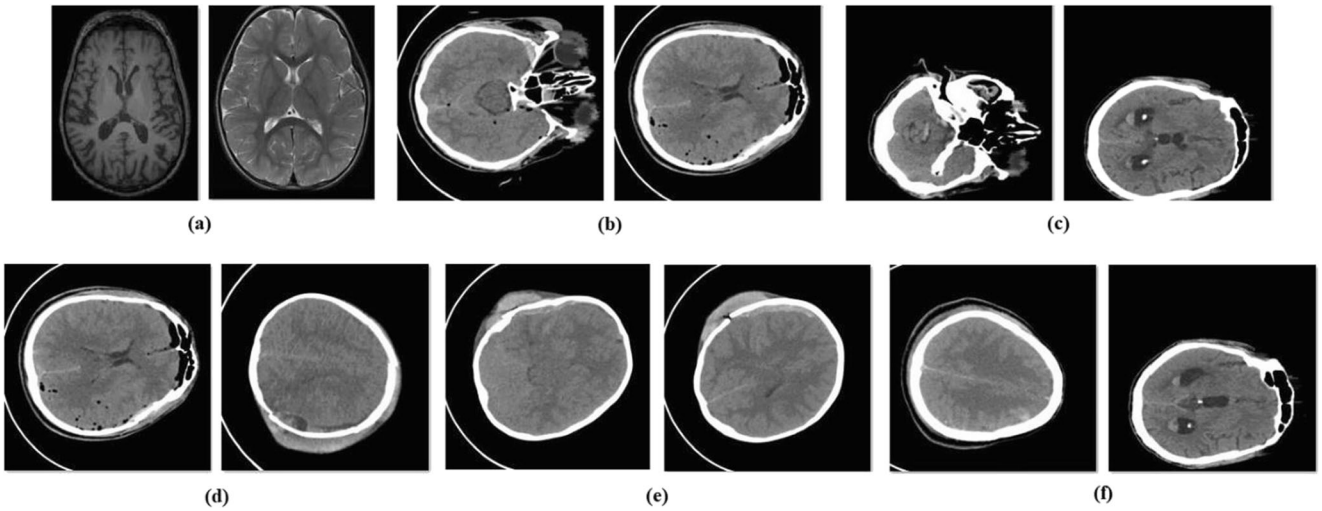

Fig. 4 Sample images. **a** No hemorrhage, **b** epidural, **c** intraventricular, **d** intraparenchymal, **e** subdural, and **f** Subarachnoid

under various classes of ICH. The dataset holds a total of 82 CT scan images of the persons with traumatic brain injury. ICH areas in the scan images are outlined in all slices using two radiologists. The CT scans of 75 subjects in NIfTI format are made public in this dataset.

The dataset is collected from the CT scans of 82 persons under the age group up to 72 years. Additionally, the dataset contains images under 6 classes such as intraventricular with 24 slices, intraparenchymal with 73 slices, subdural with 56 slices, subarachnoid with 18 slices, and no hemorrhage with 2173 slices. The outcomes are observed with respect to 4 measures such as sensitivity, specificity, accuracy, and precision. The classification results attained by the proposed model under several number of runs are provided in Table 1. For comparative study, a group of models utilized to comparison is U-Net [22], Watershed Algorithm with ANN (WA-ANN) [23], ResNexT [24], Window Estimator Module to a Deep Convolutional Neural Network (WEM-DCNN) [25], CNN, and SVM methods. The comparative results analysis of the proposed and existing models are provided in Table 2.

Figures 5 and 6 displays the ICH diagnosis of the GC-SDL model in terms of different performance measures. The figure denoted that the GC-SDL model has reached superior performance under a varying number of runs. For instance, under the run-1, the GC-SDL model has attained better ICH diagnosis results with the sensitivity of 93.45%, specificity of 97.88%, precision of 95.61%, and accuracy of 95.21%. Along with that, under the run-2, the GC-SDL method has obtained better ICH analysis results with a sensitivity of 93.89%, specificity of 97.65%, precision of 95.82%, and accuracy of 96.18%.

At the same time, under the run-3, the GC-SDL approach has achieved optimal ICH diagnosis outcomes with the sensitivity of 94.51%, specificity of 96.91%, precision of 95.99%, and accuracy of 94.90%. Simultaneously, under the run-4, the GC-SDL model has reached better ICH diagnosis outcomes with the sensitivity of 93.98%, specificity of 97.65%, precision of 95.45%, and accuracy of 95.46%. At last, under the run-5, the GC-SDL method has obtained the best ICH analysis outcomes with the sensitivity of 94.21%, specificity of 98.81%, precision of 96.08%, and accuracy of 96.92%.

Figure 7 showcases the analysis of the average result of the GC-SDL model. The figure depicted that the GC-SDL model

Table 1 Result analysis of proposed GC-SDL method on various number of runs

No. of runs	Sensitivity	Specificity	Precision	Accuracy
Run-1	93.45	97.88	95.61	95.21
Run-2	93.89	97.65	95.82	96.18
Run-3	94.51	96.91	95.99	94.90
Run-4	93.98	97.65	95.45	95.46
Run-5	94.21	98.81	96.08	96.92
Average	94.01	97.78	95.79	95.73

Table 2 Result analysis various measures on proposed GC-SDL with existing methods

Methods	Sensitivity	Specificity	Precision	Accuracy
GC-SDL	94.01	97.78	95.79	95.73
U-Net	63.10	88.60	88.19	87.00
WA-ANN	60.18	70.13	70.08	69.78
ResNexT	88.75	90.42	95.20	89.30
WEM-DCNN	83.33	97.48	89.90	88.35
CNN	87.06	88.18	87.98	87.56
SVM	76.38	79.41	77.53	77.32

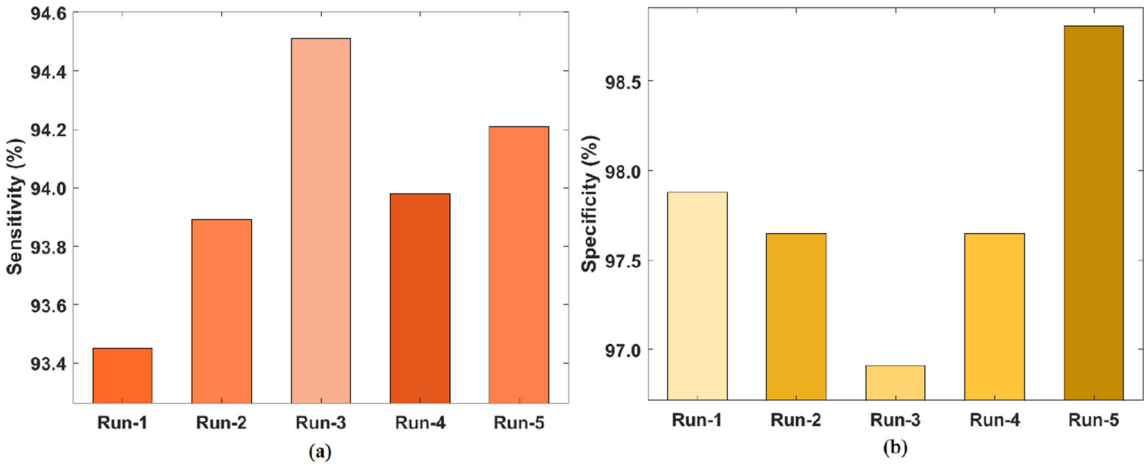

Fig. 5 Sensitivity and specificity analysis of GC-SDL model

has reached a maximum average sensitivity of 94.01%, specificity of 97.78%, precision of 95.79%, and accuracy of 95.73%.

Figure 8 illustrates the analysis of the ICH diagnosis results of the GC-SDL method with existing techniques with respect to sensitivity. The figure exhibited that the WA-ANN has appeared as the worst performer with a minimum sensitivity of 60.18%. Likewise, the U-Net approach has portrayed slightly optimal performance over the WA-ANN model with a sensitivity of 63.10%. In addition, the SVM manner has tried to demonstrate a certainly reasonable outcome with the sensitivity of 76.38%. Along with that, the WEM-DCNN and CNN methods have obtained to a moderate and closer sensitivity of 83.33% and 87.06% correspondingly. Additionally, the ResNext model has outperformed near better outcomes with the sensitivity of 88.75%. At last, the proposed GC-SDL model has achieved a maximum sensitivity of 94.01%. On the other hand, the figure also showcases the analysis of the ICH analysis outcomes of GC-SDL model with existing methods in terms of specificity. The figure demonstrated that the WA-ANN has appeared as a poor performer with the minimal specificity of 70.13%. In line with, the SVM method has showcased somewhat optimal performance over the WA-ANN model with the specificity of 79.41%. Similarly, the U-Net and CNN approaches have attained a moderate and nearer specificity of 88.6% and 88.18% respectively. Besides, the ResNext manner has tried to portray certainly reasonable results with the specificity of 90.42%. Also, the WEM-CNN model has exhibited near-optimal outcomes with the specificity of 97.48%. Finally, the projected GC-SDL method has obtained a maximum specificity of 97.78%.

Figure 9 depicts the analysis of the ICH diagnosis outcomes of GC-SDL model with existing methods with respect to precision. The figure showcased that the WA-ANN has appeared as the least performer with the minimal precision of 70.08%. At the same time, the SVM method has demonstrated slightly optimal performance over the WA-ANN method with the precision of 77.53%. Along with that, the CNN and U-Net approaches have reached to a moderate and closer precision of 87.98% and 88.19% correspondingly. Moreover, the WEM-CNN model has tried to show certainly reasonable results with the precision of 89.9%. Besides, the ResNext model has portrayed near better results with the precision of 95.2%. Finally, the proposed GC-SDL method has achieved

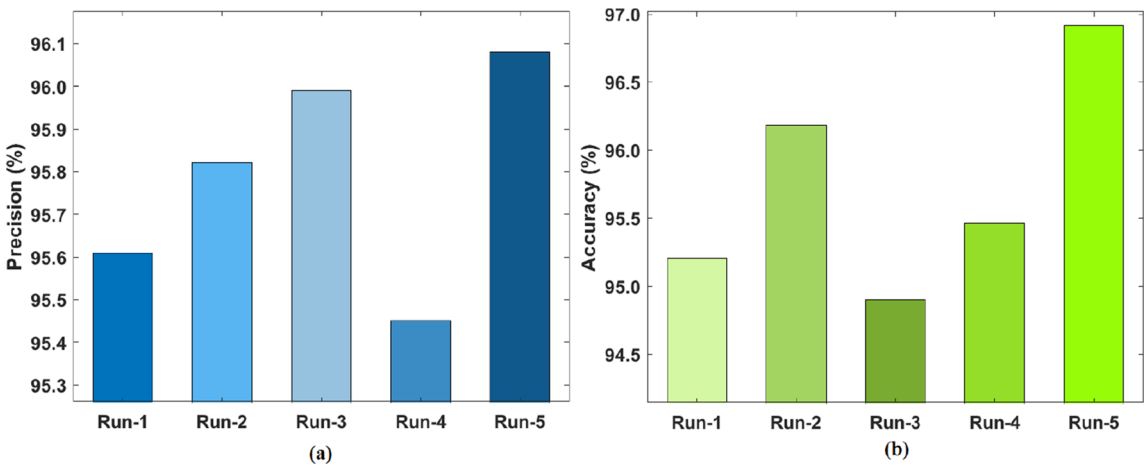

Fig. 6 Precision and accuracy analysis of GC-SDL model

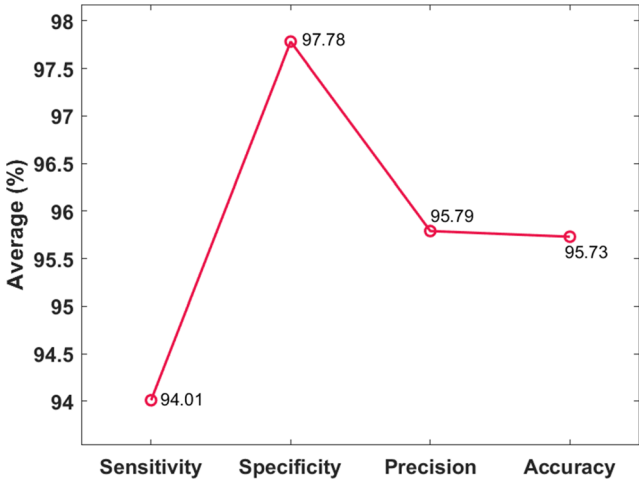

Fig. 7 Average results analysis of GC-SDL model

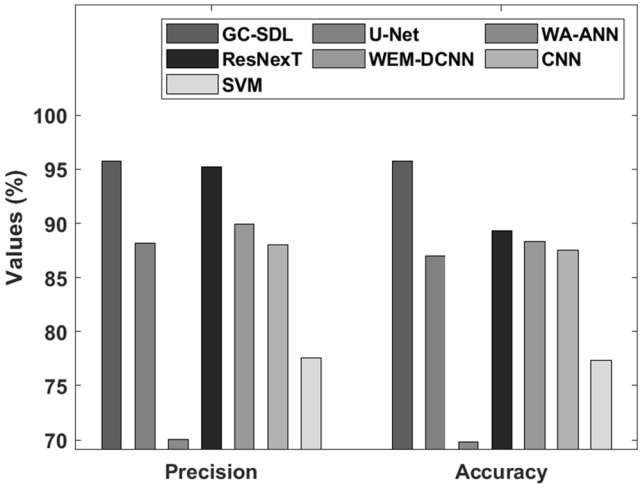

Fig. 9 Comparative results analysis of GC-SDL model in terms of precision and accuracy

the highest precision of 95.79%. The figure also demonstrates the analysis of the ICH diagnosis results of the GC-SDL model with existing methods in terms of accuracy.

The figure portrayed that the WA-ANN has appeared as the least performer with the minimal accuracy of 69.78%. Similarly, the SVM model has showcased somewhat better performance over the WA-ANN model with an accuracy of 77.32%. In line with, the U-Net and CNN models have reached a moderate and closer accuracy of 87% and 87.56% respectively. Furthermore, the WEM-CNN model has tried to exhibit a certainly reasonable outcome with the accuracy of 88.35%. Moreover, the ResNext model has demonstrated near-optimal results with an accuracy of 89.3%. Finally, the presented GC-SDL model has attained a maximum accuracy of 95.73%. The proposed method has attained better results due to the following reasons. The noise removal using GF technique acts a primary step to enhance the image quality. In addition, the GrabCut-based segmentation is useful to detect the affected regions. At last, the inclusion of the SDL model results to improved classifier results over the other methods.

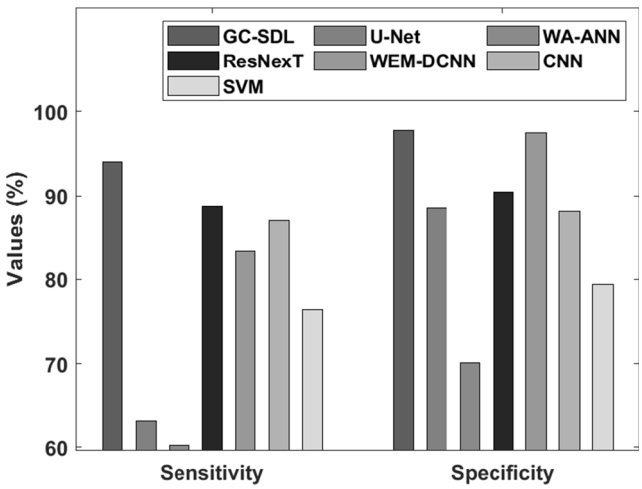

Fig. 8 Comparative results analysis of GC-SDL model in terms of sensitivity and specificity

4 Conclusion

This paper has developed a novel GC-SDL model for the detection and classification of ICH. The proposed ICH diagnosis model, named GC-SDL model comprises GF based preprocessing, GrabCut-based segmentation, SDL-based feature extraction, and SM-based classification. In the beginning, image preprocessing using the GF technique is employed as a preprocessing technique to eradicate the noise. Subsequently, segmentation and feature extraction processes are carried out. Finally, the SM layer is employed for the classification process to determine the different classes of ICH. In order to investigate the performance of the GC-SDL model, an extensive set of experimentation takes place using a benchmark ICH dataset and the results are examined under different evaluation metrics. The attained simulation results ensured the goodness of the GC-SDL model in the diagnosis of ICH. In future, advanced DL models can be employed for feature extraction and hyperparameter tuning process can be introduced to enhance the classification performance.

Authors' contribution The manuscript was written through contributions of all authors. All authors have given approval to the final version of the manuscript.

Funding Dr. K. Shankar sincerely acknowledge the financial support of RUSA–Phase 2.0 grant sanctioned vide Letter No. F. 24-51/2014-U, Policy (TNMulti-Gen), Dept. of Edn. Govt. of India, Dt. 09.10.2018.

Compliance with ethical standards

Conflict of interest The authors declare that they have no conflict of interest.

References

1. Wang C, Lai W (2019) A fuzzy model of wearable network real-time health monitoring system on pharmaceutical industry. Personal and Ubiquitous Computing, pp1–9
2. Cola, G. and Vecchio, A., 2018. Wearable systems for e-health and wellbeing. personal and ubiquitous computing, (2018) 22:225
3. Divani AA, Majidi S, Luo X, Souslian FG, Zhang J, Abosch A, Tummala RP (2011) The ABCs of accurate volumetric measurement of cerebral hematoma. Stroke 42(6):1569–1574
4. Wang S, Lou M, Liu T, Cui D, Chen X, Wang Y (2013) Hematoma volume measurement in gradient echo MRI using quantitative susceptibility mapping. Stroke 44 (8), 2315–2317 (Aug. 1)
5. Kang S, Paul A, Jeon G (2017) Reduction of mixed noise from wearable sensors in human-motion estimation. Comput Electr Eng 61:287–296
6. Ma L, Wu J, Zhang J, Wu Z, Jeon G, Zhang Y (Sept 2020) Research on sea clutter reflectivity using deep learning model in industry 4.0. IEEE Trans Industrial Informatics 16(9):5929–5937
7. Lakshmanaprabu SK, Mohanty SN, Shankar K, Arunkumar N, Ramireze G (2019) Optimal deep learning model for classification of lung cancer on CT images. Futur Gener Comput Syst 92:374–382
8. Sikkandar, M. Y., Alrasheadi, B. A., Prakash, N. B., Hemalakshmi, G. R., Mohanarathinam, A., & Shankar, K. (2020). Deep learning based an automated skin lesion segmentation and intelligent classification model. Journal of ambient intelligence and humanized computing, 1-11
9. Mohamed Elhoseny, Gui-Bin Bian, SK. Lakshmanaprabu, K. Shankar, Amit Kumar Singh, Wanqing Wu, "Effective features to classify ovarian cancer data in internet of medical things", Computer Networks, Volume 159, Pages 147–156, August 2019
10. Ahmed I, Din S, Jeon G, Piccialli F (July 2020) Exploring deep learning models for overhead view multiple object detection. IEEE Internet Things J 7(7):5737–5744
11. Prevedello LM, Erdal BS, Ryu JL, Little KJ, Demirer M, Qian S, White RD (2017) Automated critical test findings identification and online notification system using artificial intelligence in imaging. Radiology 285:923–931
12. Grewal, M.; Srivastava, M.M.; Kumar, P.; Varadarajan, S. RADnet: radiologist level accuracy using deep learning for hemorrhage detection in CT scans. In Proceedings of the 2018 IEEE 15th International Symposium on Biomedical Imaging (ISBI 2018), Washington, DC, USA, 4–7 April 2018; pp. 281–284
13. Ye H, Gao F, Yin Y, Guo D, Zhao P, Lu Y, Wang X, Bai J, Cao K, Song Q, Zhang H, Chen W, Guo X, Xia J (2019) Precise diagnosis of intracranial hemorrhage and subtypes using a three-dimensional joint convolutional and recurrent neural network. Eur Radiol 29: 6191–6201
14. Lee H, Yune S, Mansouri M, Kim M, Tajmir SH, Guerrier CE, Ebert SA, Pomerantz SR, Romero JM, Kamalian S, Gonzalez RG, Lev MH, Do S (2019) An explainable deep-learning algorithm for the detection of acute intracranial haemorrhage from small datasets. Nat Biomed Eng 3:173–182
15. Chang P, Kuoy E, Grinband J, Weinberg B, Thompson M, Homo R, Chen J, Abcede H, Shafie M, Sugrue L et al (2018) Hybrid 3D/2D convolutional neural network for hemorrhage evaluation on head CT. Am J Neuroradiol 39:1609–1616
16. Jnawali, K.; Arbabshirani, M.R.; Rao, N.; Patel, A.A. Deep 3D convolution neural network for CT brain hemorrhage classification. In Medical Imaging 2018: Computer-Aided Diagnosis; International Society for Optics and Photonics: Washington, DC, USA, 2018; Volume 10575, p. 105751C
17. Arbabshirani MR, Fornwalt BK, Mongelluzzo GJ, Suever JD, Geise BD, Patel AA, Moore GJ (2018) Advanced machine learning in action: identification of intracranial hemorrhage on computed tomography scans of the head with clinical workflow integration. NPJ Digit Med 1:9
18. Chang PD, Kuoy E, Grinband J, Weinberg BD, Thompson M, Homo R, Chen J, Abcede H, Shafie M, Sugrue L, Filippi CG (2018) Hybrid 3D/2D convolutional neural network for hemorrhage evaluation on head CT. Am J Neuroradiol 39(9):1609–1616
19. Majumdar, A., Brattain, L., Telfer, B., Farris, C. and Scalera, J., 2018, July. Detecting intracranial hemorrhage with deep learning. In 2018 40th annual international conference of the IEEE engineering in medicine and biology society (EMBC) (pp. 583-587). IEEE
20. K. Shankar, Abdul Rahaman WahabSait, DeepakGupta, S.K.Lakshmanaprabu, Ashish Khanna, Hari Mohan Pandey, "Automated detection and classification of fundus diabetic retinopathy images using synergic deep learning model", Pattern Recognition Letters, Volume 133, Pages 210–216, May 2020
21. https://physionet.org/content/ct-ich/1.3.1/
22. Hssayeni, M.D., Croock, M.S., Salman, A.D., Al-khafaji, H.F., Yahya, Z.A. and Ghoraani, B., 2020. Intracranial hemorrhage segmentation using a deep convolutional model. Data, 5(1), p.14
23. Davis, V. and Devane, S., 2017, December. Diagnosis & classification of brain hemorrhage. In 2017 international conference on advances in computing, communication and control (ICAC3) (pp. 1-6). IEEE
24. Danilov G, Kotik K, Negreeva A, Tsukanova T, Shifrin M, Zakharova N, Batalov A, Pronin I, Potapov A (2020) Classification of intracranial hemorrhage subtypes using deep learning on CT scans. Studies in Health Technology and Informatics 272:370–373
25. Karki M, Cho J, Lee E, Hahm MH, Yoon SY, Kim M, Ahn JY, Son J, Park SH, Kim KH, Park S (2020) CT window trainable neural network for improving intracranial hemorrhage detection by combining multiple settings. Artificial Intelligence in Medicine, p 101850